

# Wearable Power-Textiles by Integrating Fabric Triboelectric Nanogenerators and Fiber-Shaped Dye-Sensitized Solar Cells

Xiong Pu, Weixing Song, Mengmeng Liu, Chunwen Sun, Chunhua Du, Chunyan Jiang, Xin Huang, Dechun Zou,\* Weiguo Hu,\* and Zhong Lin Wang\*

Electronic-textile (E-textile) or smart textile, which integrates multifunctional electronic/optoelectronic devices into fashionable/stylish clothing, holds great promise for the next growth of the market of wearable electronics.<sup>[1]</sup> Various components of electronic devices have been demonstrated in smart garments or fabrics, including textile circuits,<sup>[2]</sup> light emitting diodes (LED),<sup>[3]</sup> and a variety of sensors for temperature,<sup>[4]</sup> pressure,<sup>[5]</sup> medical diagnosis,<sup>[6]</sup> etc. Still, an energy device is required to power the E-textile, while the conventional bulky batteries fall short of the required flexibility, comfort, and lightweight for the textile. Thereby, tremendous efforts have been made to design energy storage devices (batteries or supercapacitors) into fibers or fabrics.<sup>[7]</sup> Despite the unsolved issues of low energy density and safety, frequently recharging of these devices raises the inconvenience. An alternative solution is integrating flexible energy-generating devices into the E-textile, to either provide direct power source or sustain the energy storage devices.

Fiber-shaped energy-generating devices present attractive prospects and unique advantages for the applications in E-textiles, considering that 1D fiber is the building block of textiles.<sup>[8]</sup> Among them, the fiber-shaped dye-sensitized solar cells (FDSSCs) have attracted increasing attentions in recent years due to the high power output and low fabrication cost.<sup>[9]</sup> Their lightweight, flexibility, and 3D light-harvesting capability also promise their applications in rapidly developing fields of wearable self-powered electronic devices. Moreover, they can be easily woven into fabrics, and they show the same photovoltaic performances with the flat solar cells.<sup>[10]</sup> The FDSSCs

have been developed mainly based on TiO<sub>2</sub> nanoparticles with the efficiency of more than 7% and have good stability under deformation.<sup>[11,12]</sup>

Considering that solar energy is dependent on the weather and people stay most of a day indoors, mechanical energy could be an appropriate complement due to its universal availability. The triboelectric nanogenerator (TENG),<sup>[13,14]</sup> coupling the effect of contact-electrification and electrostatic induction, has been demonstrated to be versatile in scavenging different types of mechanical energies, ranging from vibration,<sup>[15]</sup> wind,<sup>[16]</sup> water wave,<sup>[17]</sup> to human motions.<sup>[18–20]</sup> The abundant choice of materials and structure designs of the TENG enable its feasibility in integration with the E-textile for harvesting energy from human motions. Silver coating,<sup>[21]</sup> carbon nanotubes,<sup>[22]</sup> and carbon fiber<sup>[23]</sup> were applied to textile fibers, functioning as the electrode of the textile-based or fiber-based TENG. In our previous studies, a woven TENG textile was realized by electroless deposition (ELD) of conformal and low-cost nickel coating to convert textile yarns/fabrics into conductive electrodes.<sup>[24]</sup> Despite these preliminary findings, further research is still required to improve the output power of the TENG textile. Meanwhile, integration of the whole textile-based TENG and solar cell has seldom been found in literature, though several previous works have been reported integrated devices on flat substrates.<sup>[25]</sup>

Herein, we developed a grating-structured TENG fabric and its integration with FDSSCs so as to achieve a whole textile-based energy harvesting system. A route of laser-scribing masking and ELD Ni plating was first proposed for the synthesis of conductive circuits/patterns on the textile. Interdigitated grating-structured TENG fabrics were then fabricated in aim to convert low-frequency human motion energy into high-frequency current outputs. By reducing the grating size, large improvements were achieved in the current amplitude and output power. Furthermore, FDSSCs and TENG fabrics were integrated together into a cloth as complementary power devices for harvesting both the energy of sunshine and human motions.

The energy-generating device for wearable electronics or E-textiles should be versatile for fashionable and comfortable designs. Whereas, most of the previous reported TENGs for biomechanical energy-harvesting lack this versatility. The ideal TENG for E-textiles is in the form of fabrics. As schemed in **Figure 1a**, a power-textile can be designed with the fabrics of the sleeve and underneath the arm (herein after noted as slider fabric and stator fabric, respectively) functioning as two pairs

Dr. X. Pu, Dr. W. X. Song, M. M. Liu, Prof. C. W. Sun,  
Dr. C. H. Du, C. Y. Jiang, X. Huang, Prof. D. C. Zou,  
Prof. W. G. Hu, Prof. Z. L. Wang  
Beijing Institute of Nanoenergy and Nanosystems  
Chinese Academy of Sciences  
National Center for Nanoscience and Technology  
(NCNST)  
Beijing 100083, China  
E-mail: dczou@pku.edu.cn; huweiguo@binn.cas.cn; zlwang@gatech.edu

Prof. D. C. Zou  
College of Chemistry and Molecular Engineering  
Peking University  
Beijing 100871, China

Prof. Z. L. Wang  
School of Materials Science and Engineering  
Georgia Institute of Technology  
Atlanta, GA 30332-0245, USA



DOI: 10.1002/aenm.201601048

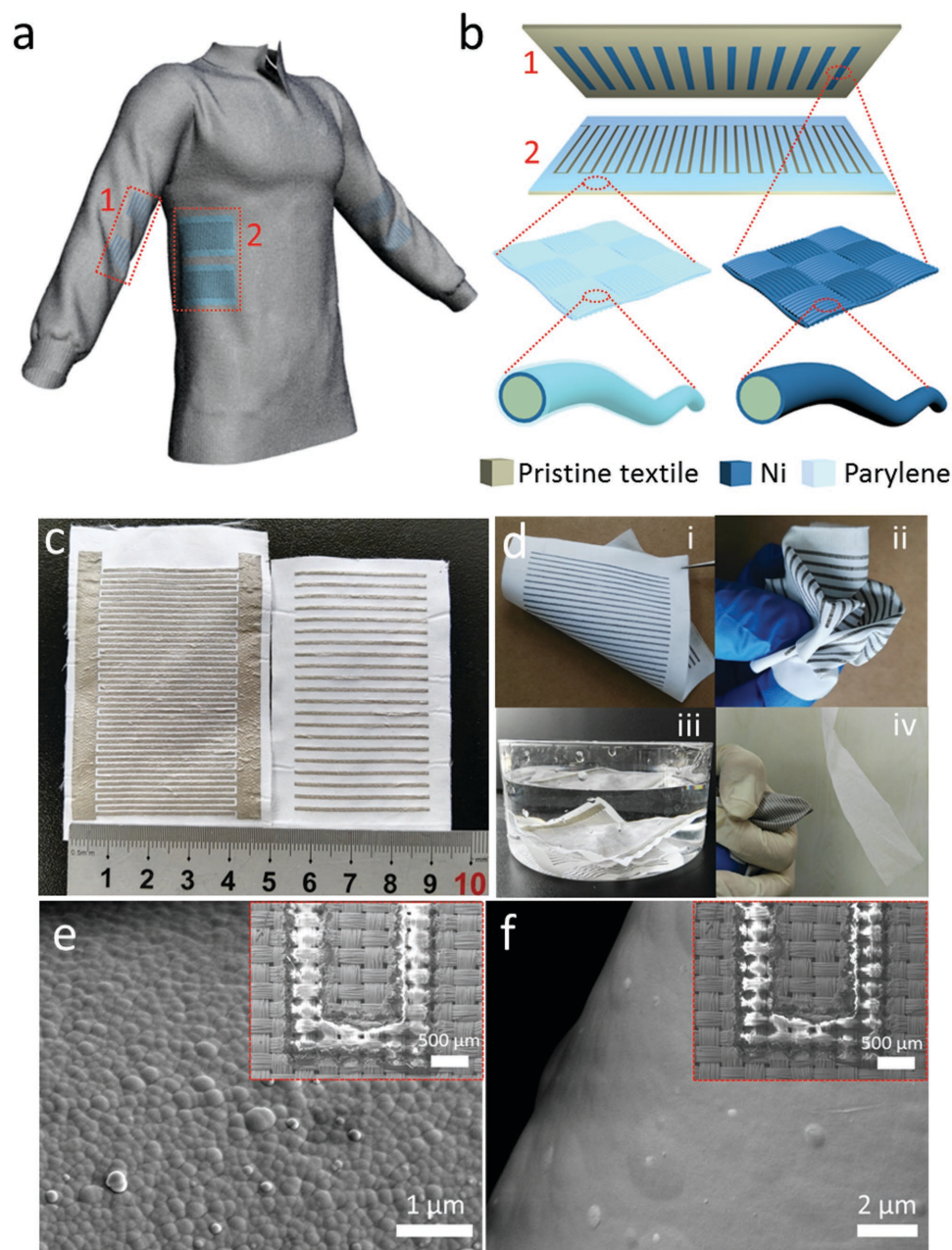


**Figure 1.** The fabrication of TENG fabrics. a) The scheme of a power-textile with a pair of TENG fabrics consisting of a slider fabric (1) in the sleeve and a stator fabric (2) underneath the arm. b) The scheme of the configuration of the TENG fabrics. c) A photo of a pair of TENG fabrics. d) The photos showing the flexibility (i), softness (ii), washability (iii), and breathability (iv) of the TENG fabrics. SEM images showing the surface of e) Ni coating and f) parylene coating. The inset in panels (e) and (f) shows the interdigitated electrode on a stator fabric without and with parylene coating, respectively.

of sliding-mode TENGs, which scavenge the swing energy of two arms during walking or running. The structure of a pair of TENG fabrics is depicted in Figure 1b. The stator fabric under the arm has two metal electrodes with interdigitated configuration; the slider fabric has a series of parallel grating segments, of which the number, size, and spacing are identical to that of one electrode under the arm. It should be noted that all of the metal electrodes/segments consist of woven fibers with conformal Ni coatings. For the stator fabrics, an additional layer of parylene is applied on the top of Ni by chemical vapor deposition (CVD),

which serves as an electrification layer when it contacts with the parallel Ni segments and has relative friction.

To fabricate the TENG fabrics, a route of laser-scribing masking was developed, as schemed in Figure S1a (Supporting Information). A polyester fabric sealed with commercial Kapton tape on both sides was put underneath a laser for drawing intended patterns as mask for subsequent ELD plating of Ni. The intensity of laser was adjusted not to damage the sandwiched polyester fabric. After coating the exposed textile with Ni film, the Kapton tape was then detached, yielding a conductive pattern

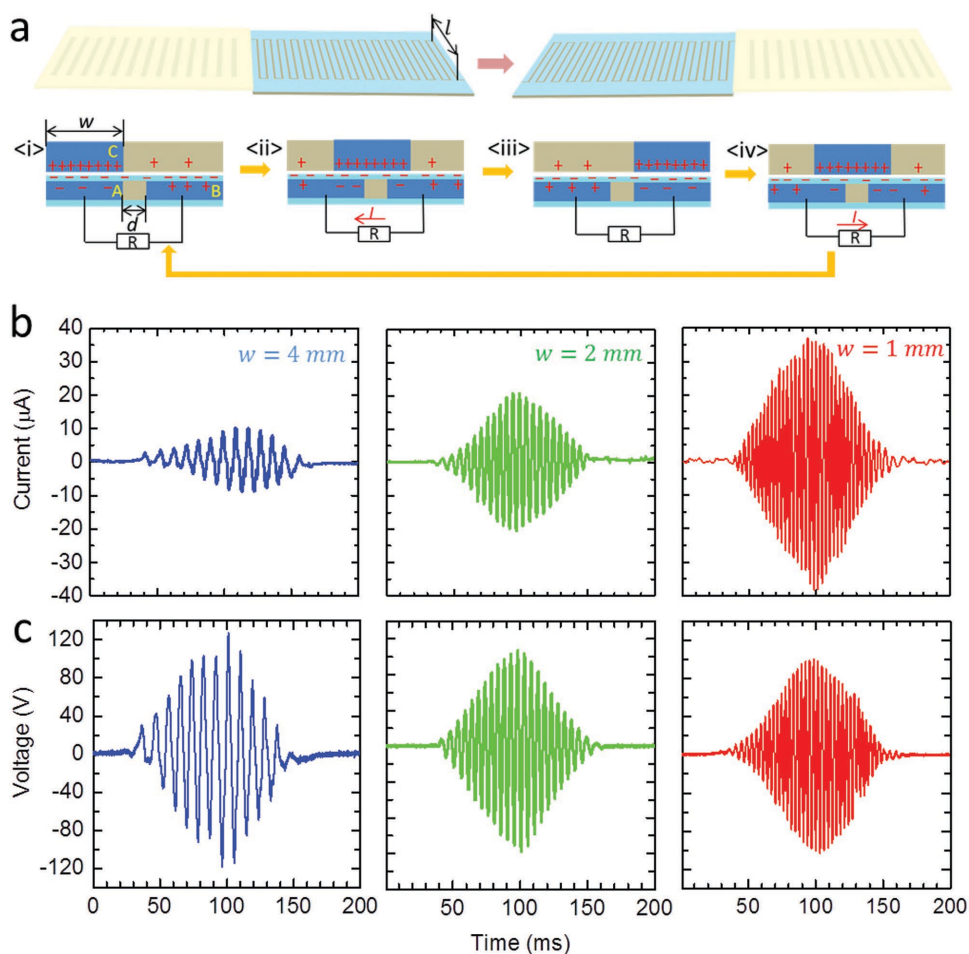
of Ni film on one side of the fabric. This route is promising for synthesis of textile circuits. For demonstration, three different conductive drawings were fabricated on a polyester fabric, i.e., a pentagram, a target, and an array of  $1 \times 1$  mm squares (see Figure S1b, Supporting Information). Figure S1c (Supporting Information) shows a purple LED bulb lighted by a DC current source through a simple conductive circuit on a fabric.

Figure 1c is a pair of TENG fabrics derived from a white polyester cloth. Each electrode has 21 grating segments, and the segment dimension and spacing is  $1 \times 35$  mm and 0.5 mm, respectively. The thin coating of Ni does not significantly increase the weight of the fabric, maintaining the lightweight and softness of the pristine textile.<sup>[26]</sup> As demonstrated in Figure 1d, the TENG fabrics can be easily bent, wrapped, and immersed in water without damage, indicating their excellent flexibility and capability for washing with household laundry. Furthermore, an air gun, wrapped by a stator fabric with both interdigitated Ni electrodes and parylene layer, is still able to blow a tissue, suggesting the breathability of the TENG fabrics. The TENG fabrics were completely folded for  $180^\circ$  for 100 times (Figure S3a, Supporting Information), washed by a household laundry for 20 min. (Figure S3b, Supporting Information), and then ironed to be flat again (Figure S3c, Supporting Information). The output

short-circuit current at sliding speed of  $0.25 \text{ m s}^{-1}$  shows no significant decrease after undergoing these harsh deformations (Figure S3d, Supporting Information), confirming that the TENG fabrics are flexible and washable. These features, seldom reported in previous energy-generating textiles,<sup>[21,27]</sup> are crucial for the realization of comfortable power-textile in commercial garments.

The ELD Ni coating is a conformal layer of Ni nanoparticles wrapping up the polyester fiber (see Figure 1e). After the parylene coating, a smooth layer of parylene can be observed (see Figure 1f). The nanoscale roughness of the Ni film can benefit the output power of the TENG due to the improved surface charge density.<sup>[28]</sup> Both the ELD coating of Ni and the CVD coating of parylene reserve the woven structure of the pristine textile and interstitials among the fibers (see Figure S2, Supporting Information), further confirming the flexibility and breathability of the TENG fabrics. The insets in Figure 1e,f show the 0.5 mm spacing between two Ni segments after the coating of Ni and parylene, respectively, indicating the clean edge without any shortening of two electrodes.

The relative sliding between the slider and stator fabric can generate alternative electricity between two electrodes in the stator fabric. The operational mechanism of the TENG fabrics is schematically illustrated by a basic unit in Figure 2a.



**Figure 2.** The working mechanism of TENG fabrics. a) The scheme of the working mechanism of the TENG fabrics. The output b) short-circuit current and c) open-circuit voltage of three sets of TENG fabrics with different segment sizes, i.e.,  $w = 4, 2,$  and  $1$  mm.

The wavy woven fabrics are simplified as flat films. The direct contact between the Ni segments in the slider fabric with the parylene layer in stator fabric leads to the electrification, with the parylene negatively charged and Ni positively charged. Naked polyester fabric can also have electrification with underneath parylene layer, but it is far less tribo-positive than Ni.<sup>[14]</sup> Therefore, for charge conservation, the charge density in parylene layer (noted as  $\sigma$ ) is almost half of that in Ni segments in the slider fabric, since the area of each segment is the same. At the initial state (i), the Ni segment C is aligned with the electrode A, leading to the accumulation of negative charges in electrode A and positive charges in electrode B, due to the electrostatic induction. As the slider fabric moves forward to electrode B (state (ii)), electric current flows from electrode B to A through the external circuit, so as to maintain the local charge conservation. When the slider fabric is aligned with electrode B (state (iii)), the charge polarity of electrode A and B is reversed. If the slider fabric keeps moving forward (state (iv)), the current flows in the opposite direction until the Ni segment C gets back to be aligned with electrode A. The total charges transferred for a single transport process can be approximated to be:  $\Delta Q = n\sigma(w+d)l$ , where  $n$  is the number of involved Ni segments in slider fabrics,  $d$  is the gap between the two interdigitated electrodes,  $w$  and  $l$  is the width and length of each segment, respectively. The corresponding peak short-circuit current is thereby estimated to be  $I = \frac{\Delta Q}{\Delta t} = n\sigma vl$ , where  $v$  is the velocity of the slider fabric. The frequency of the alternative current can be derived as  $f = \frac{v}{2(d+w)}$ <sup>[29]</sup>

According to the above analysis and previously reported works,<sup>[19,30]</sup> reducing the size of unit segment can efficiently

improve the output current and frequency. Three sets of TENG fabrics were fabricated with the gap fixed at 0.5 mm and the segment width  $w$  varied to be 4, 2, and 1 mm, respectively. To obtain the same device area, corresponding segment number  $n$  of a single electrode is 7, 12, and 21, respectively. We define that one sliding cycle starts when the slider fabric reaches the stator fabric, and ends when it slides out of the slider fabric, as schemed in Figure 2a. Therefore, for each sliding cycle, the tribo-charges will transfer for  $(2n-1)$  times, generating  $(2n-1)$  cycles of AC current, which can be confirmed by the measured short-circuit current as shown in Figure 2b. The rhomboidal shape of the current during a one-way sliding cycle is due to the increasing–maximizing–decreasing variation of the contact area, and thus the same variation of segment number and tribo-charge amount involved in a charge-transfer process. The corresponding maximum current of the three TENG fabrics sliding at 0.5 m s<sup>-1</sup> was measured to be 10, 20, and 37  $\mu$ A, respectively, close to a linear increase with the segment number. The open-circuit voltage  $V_{OC}$  shows the same alternative features with the current, but the maximum amplitude slightly decreases with reducing the segment width (see Figure 2c). The open-circuit voltage in TENG can be written as:  $V_{OC} = \frac{\Delta Q}{C}$ ,<sup>[19]</sup> where  $C$  is the capacitance of interdigitated electrodes. By dividing electrodes into smaller segments,  $\Delta Q$  have ignorable change, but the capacitance  $C$  increases, leading to the slightly lower  $V_{OC}$ .<sup>[31]</sup> The continued sliding of TENG fabrics back-and-forth can generate a series of rhomboidal output pulses as shown in Figure S4a (Supporting Information). An elongated test for more than 1200 sliding cycles of the TENG fabrics was shown in Figure S4b (Supporting Information), indicating no obvious degradation of the TENG fabrics. Since the TENG fabrics are

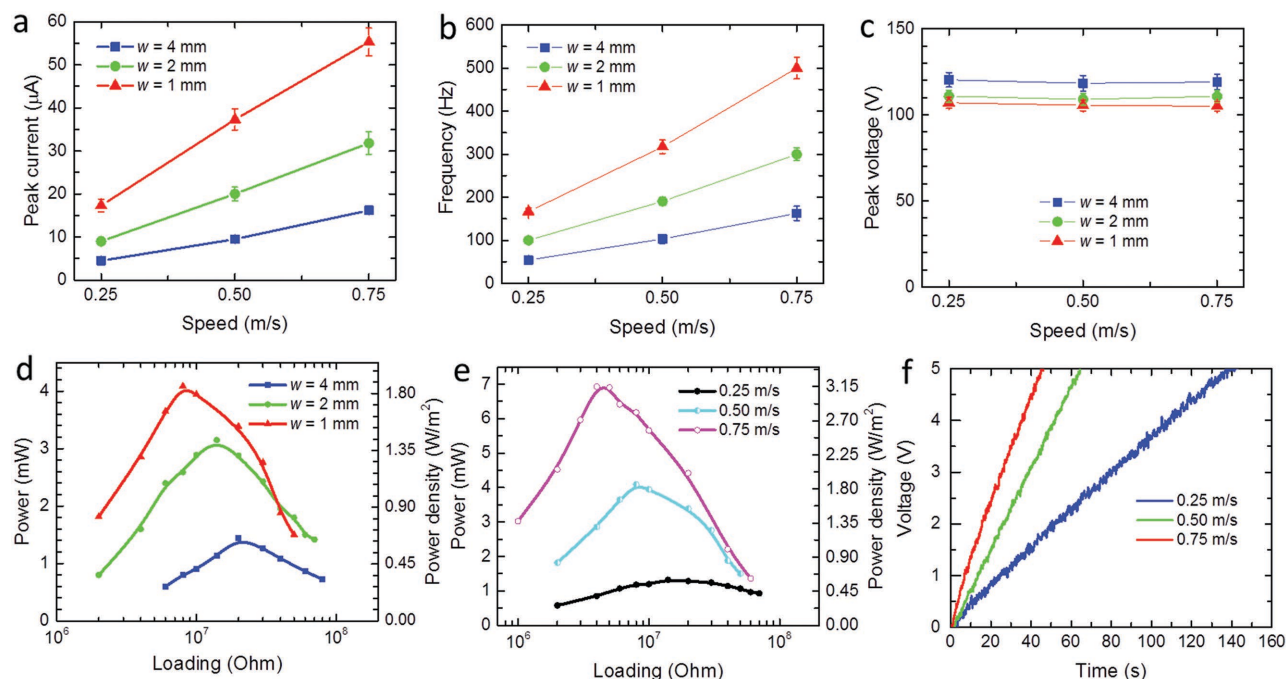


**Figure 3.** The optimization of the structure of TENG fabrics. The summarized maximum amplitude of a) short-circuit current, b) frequency, and c) maximum amplitude of open-circuit voltage of the three sets of TENG fabrics at different sliding speeds. d) The variation of the output power of the three sets of TENG fabrics with the external loading resistance. e) The output power of the TENG fabric ( $w = 1$  mm) at different sliding speeds. f) The charging of a 2.2  $\mu$ F capacitor by the TENG fabric ( $w = 1$  mm) at different sliding speeds.

developed from the same polymeric materials of common clothes, the wear resistance is believed to be comparable with ordinary clothes. But, cautions must be paid to the connection wires or other circuit components in the real applications, since the poor contact may lead to the failure of the device.

The capability of our TENG fabrics in converting low-frequency human motion into high-frequency current output should be noted. First, each sliding of the slider fabric generates multiple current peaks rather than one single peak by TENG with contact-separation mode,<sup>[17]</sup> leading to a higher output energy and mechanical-to-electrical energy conversion efficiency.<sup>[26]</sup> Second, the generated AC current at high frequency can readily be managed by a conventional coil transformer, so that achieved impedance matching between the TENG fabric and external loading improves the energy utilization efficiency.<sup>[32]</sup> As shown in Figure S5 (Supporting Information), the short-circuit current transformed by a transformer with 10:1 coil ration is about sevenfold higher than that of the pristine TENG fabric.

Velocity is another important factor for the output of the TENG fabrics. Both the current and frequency increase linearly with the speed of the slider fabric (see Figure 3a,b), which makes the grating-structured TENG an excellent speed sensor.<sup>[33]</sup> For TENG fabric with 1 mm wide segment, the frequency can be about 500 Hz (see Figure 3b) and the amplitude of peak current reaches about 55  $\mu\text{A}$  (see Figure 3a) at 0.75  $\text{m s}^{-1}$  sliding speed, much higher than that of previously reported textile-based TENGs. On the contrary, the amplitude of open-circuit voltage almost keeps constant with the sliding speed, since both the  $\Delta Q$  and  $C$  are independent to the sliding velocity (see Figure 3c). External resistance connected with the TENG fabrics was varied to obtain the maximum output power. It can be observed that significant improvement in output power and decrease in matched external resistance can be achieved by reducing the segment width or increasing the sliding speed (see Figure 3d,e, respectively), accordant with previously reported theoretical analysis.<sup>[31]</sup> The maximum output power density is about 1.9  $\text{W m}^{-2}$  with 8 MOhm resistor for  $w = 1$  mm, but only 0.7  $\text{W m}^{-2}$  with 20 MOhm resistor for  $w = 4$  mm, at sliding speed of 0.5  $\text{m s}^{-1}$  (see Figure 3d). For the TENG fabric with 1 mm wide segment, the maximum power density can be about 0.6  $\text{W m}^{-2}$  even at low sliding speed of 0.25  $\text{m s}^{-1}$ , which rises to about 3.2  $\text{W m}^{-2}$  at speed of 0.75  $\text{m s}^{-1}$ . The alternative current of the TENG fabric with 1 mm wide segment was rectified to charge a 2.2  $\mu\text{F}$  capacitor (see Figure 3f). The voltage increases to 5 V in 140 s when sliding at 0.25  $\text{m s}^{-1}$ , and in 45 s when sliding at 0.75  $\text{m s}^{-1}$ .

According to the above results, it can be concluded that high output performances can be achieved by the TENG fabric with grating structure and small segment size. Therefore, a pair of TENG fabrics with 1 mm wide segments was knitted onto a common cloth to confirm its viability in real working situation, as shown in Figure 4a. A liquid crystal display (LCD) panel can be easily lighted up by swinging the slider fabric under the arm (see the inset in Figure 4ai). Meanwhile, the relative friction of the slider and stator fabric can light 20 green LED bulbs (see Figure 4aii) and a 5  $\times$  2.5 cm LCD panel with characters of "binn" (see Figure 4aiii). Rectified short-circuit current of the TENG fabrics at different speed of human motion was

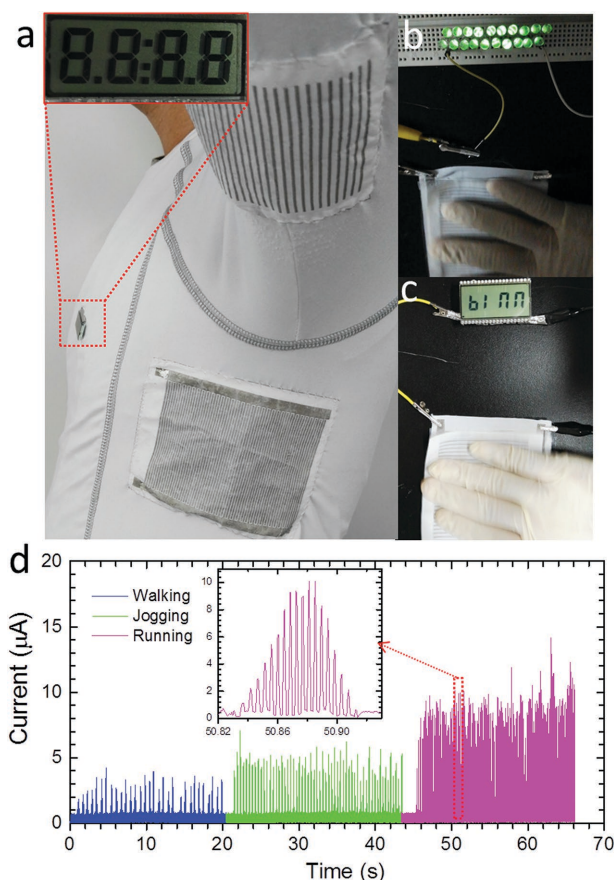


**Figure 4.** The demonstration of TENG fabrics. a) A photo of a power-textile with a pair of TENG fabrics, which can light up a LCD panel (the inset). The photo showing b) 20 green LEDs and c) a LCD panel lighted by a pair of TENG fabrics. d) The rectified current of the TENG fabrics at different speeds of human body. The inset shows the current of one sliding cycle of the TENG fabrics.

recorded in Figure 4b. Average peak current about 3, 5, and 10  $\mu\text{A}$  was obtained for walking, jogging, and running, respectively. The smaller current amplitudes than that measured with linear motor are due to the wavy feature of human body and thereby the smaller contact surface area of the TENG fabrics. Different from TENG textile with contact-separation mode that only a single current peak was derived for one swinging of the arm,<sup>[24]</sup> a triangle current curve with multiple peaks was generated by our grating-structured TENG fabrics (see the inset in Figure 4b), transferring larger amount of charges through the external circuit.

The effect of humidity on the TENG fabrics must be considered. According to our previous experiments<sup>[16]</sup> and other reported data,<sup>[34]</sup> lower output current was observed at high relative humidity. According to experiments in our lab,<sup>[16]</sup> the current amplitude, when relative humidity (RH) is higher than RH 66%, is about only 1/3 of that at about RH 10%. At RH 50% the current is about 2/3 of that at RH 10%. Selecting highly hydrophobic surface coatings can alleviate the decrease of the output current at high humidity.<sup>[35]</sup> In this work, the experiments were conducted in an indoor environment of humidity about RH 40%. Taking Beijing for example, the yearly averaged humidity

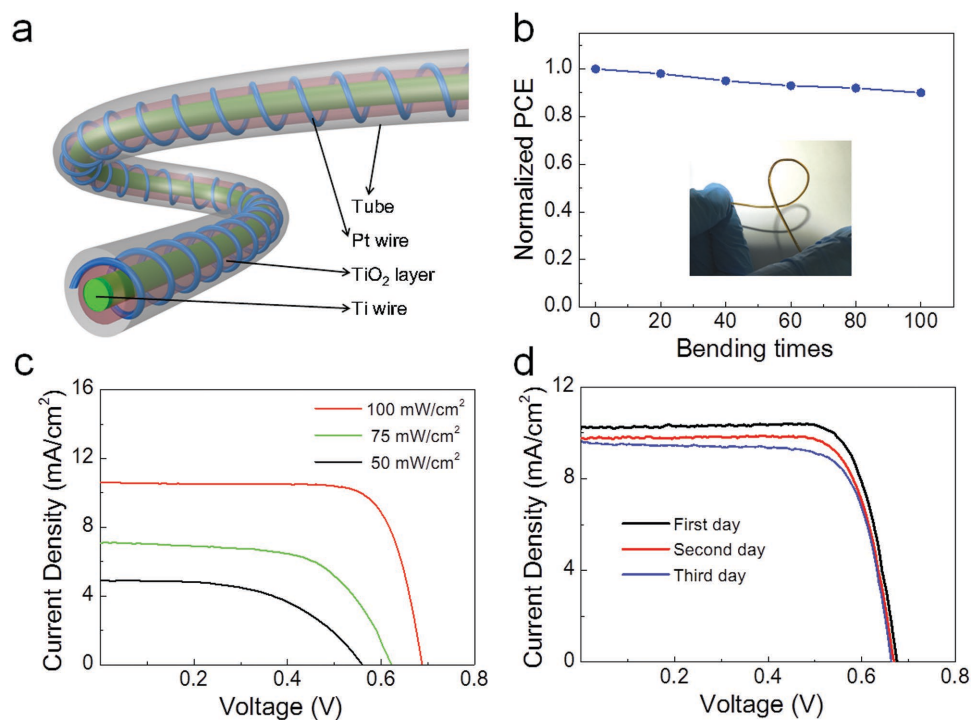


**Figure 5.** Fiber-shaped dye-sensitized solar cell (FDSSC). a) The scheme of the structure of a FDSSC. b) Relationship between the PCEs of the FDSSCs with the bending times. The inset image is the photo of a bending FDSSC. c) The current density–voltage curves of a FDSSC under different incident light intensity. d) The current density–voltage curves of the typical FDSSCs which were kept for different periods after fabrication, and the inset table is the photovoltaic performance parameters of these DSSCs.

is 54.1%, but the average humidity in July can be as high as  $\approx 70\%$ ; while in February humidity is averaged at  $\approx 40\%$ . Therefore, we expect about a 1/3 drop of the current in summer for TENG textile. But, the sunshine in summer is far more intensive than winter, and the energy-generating devices discussed hereafter (i.e., solar cell) will have larger output, which probably can also explain why solar cell and TENG textile are two good complementary power sources.

Considering that 1D fiber is the building block of a textile, FDSSCs were designed so that it can be woven or sewed into a cloth. As shown by the scheme of a FDSSC in **Figure 5a**, the fiber photoanode of the FDSSCs, composed of a Ti wire coated by mesoporous  $\text{TiO}_2$  layer, was wrapped by a twisted Pt wire serving as the counter electrode. Electrolyte was filled and sealed by a transparent PTFE tube. The Ti wire was covered by the  $\text{TiO}_2$  nanoparticles mesoporous layer (Figure S6, Supporting Information), the thickness of which can be tuned by controlling the absorbing times. The thicker mesoporous layer can absorb more dye molecules, but the nanoparticles in the thick layers above  $25\ \mu\text{m}$  lead to peel off. Therefore, there is a balance between stability and high performance for the FDSSCs. By comparison, the optimal thickness of the nanoparticles layer is  $13\text{--}23\ \mu\text{m}$ . It should be noted that the Pt wire can be replaced with inexpensive materials such as carbon fibers and steel wires to lower the cost of the device at the slight expense of the performances, as we reported previously.<sup>[36]</sup>

The photoanode and the counter electrodes of the FDSSCs were twisted together, so the devices present good flexibility,

and can be bended for many cycles without damage due to the flexibility of all the wire components. **Figure 5b** shows that the typical performance of FDSSCs decreases slightly with the bending times under bending radius of  $\approx 2\ \text{cm}$ . After bending for 100 times, the FDSSCs can maintain about 90% power conversion efficiency (PCE) of that without bending. During photovoltaic applications, light intensity is an important factor for the performance of the FDSSCs. As shown in **Figure 5c**, the current density–voltage curves of the FDSSCs were compared under different light intensities. The short-circuit current density increases with the increase of the light intensity. The open-circuit voltage also presents a similar changing trend. The incident light intensity directly affects the PCE. Under an AM 1.5 solar ( $100\ \text{mW cm}^{-2}$ ), the FDSSCs have an average PCE of 6% with a  $J_{\text{sc}}$  of about  $10.6\ \text{mA cm}^{-2}$  and a  $V_{\text{oc}}$  of 0.68 V on average. One advantage of FDSSC is that it can be easily sealed due to the smaller sealing area than that of the planar devices, i.e., only two ends of the sealing tube, which could improve the stability of the device.<sup>[11b]</sup> By comparing the  $J$ – $V$  curves and photovoltaic performance parameters of the DSSCs which were kept for different periods after fabrication (**Figure 5d**), it can be found that the well-sealed FDSSCs show stable photovoltaic performance after 10 d, and can still obtain above 5.0% conversion efficiency. Also, according to previous reports, the well-sealed dye-sensitized solar cells have passed the humidity test without major degradation and the humidity has no obvious influence on the long-term stability of devices.<sup>[37]</sup> Moreover, the fiber-shaped solar cells have very excellent stability and durability, considering the fact that the devices fabricated 1 year ago

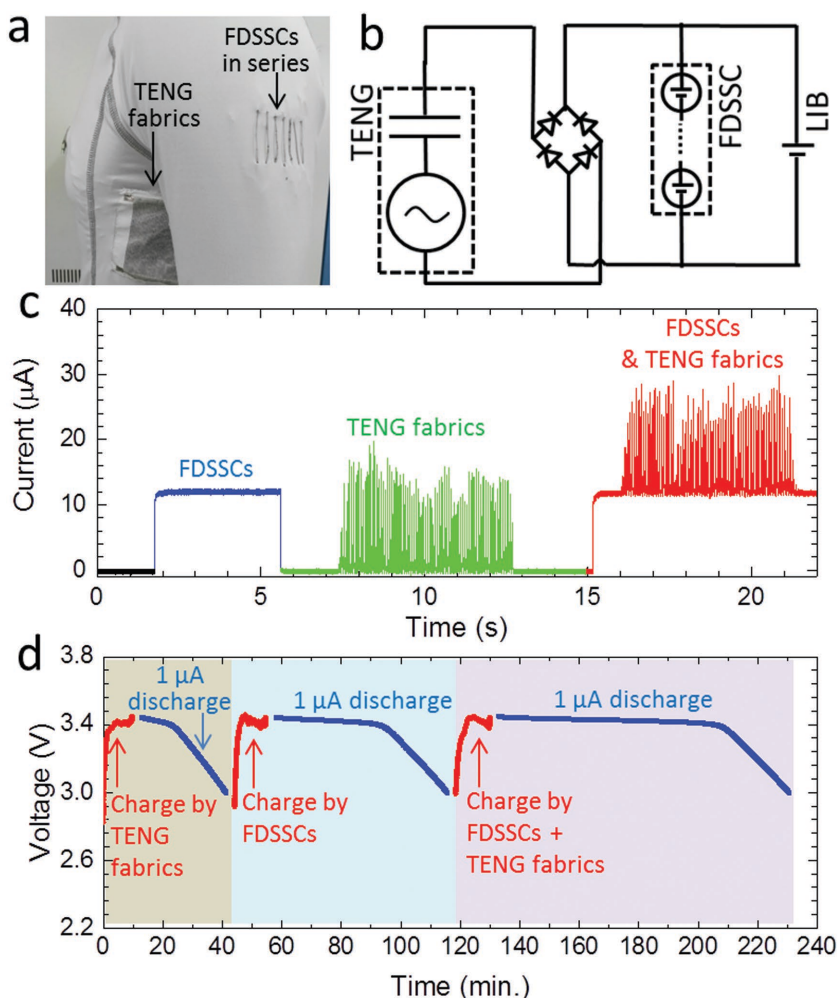


**Figure 6.** The integrated power-textile. a) A photo of a power-textile with a pair of TENG fabrics underneath the arm and seven FDSSCs in series on the shoulder. b) An equivalent circuit of a self-charging system with hybrid TENG fabrics and FDSSCs as energy-harvesting devices and LIB as energy storage device. c) The short-circuit current of FDSSCs, TENG fabrics, and the hybrid energy-harvesting device. d) The voltage profile of a LIB charged by the three energy-harvesting devices for 10 min, and corresponding discharge at  $1 \mu\text{A}$  constant current.

still present a  $V_{oc}$  of about 0.5 V, and a  $J_{sc}$  of about  $6 \text{ mA cm}^{-2}$ . Therefore, we estimate that the FDSSC pack sewed on the cloth can work for at least 6 months with effective efficiency.

The 1D FDSSCs and TENG fabrics are both facile to be integrated into a textile. For demonstration, 7 FDSSCs in series and one pair of TENG fabrics were sewed on the fabric of a common cloth (see Figure 6a). In most cases, the energy generated by the TENG fabrics and FDSSCs still needs to be stored in a battery for stable power supply for wearable electronics or E-textiles. Figure 6b shows an equivalent circuit of a self-charging system, consisting of a FDSSC pack, a TENG fabric, and a lithium-ion battery (LIB). The solar cell pack of 7 FDSSCs in series can generate an output voltage of about 5 V, which is then connected with a rectified TENG fabric in parallel so as to increase the charging current to the LIB. The FDSSC pack has a stable DC short-circuit current of about  $12 \mu\text{A}$  under the simulated solar incidence; the rectified TENG fabrics generate a short-circuit current with average maximum peak amplitude

of about  $\approx 13 \mu\text{A}$ ; while the hybrid energy-generating pack outputs an additive short-circuit current (see Figure 6c). An LIB coin cell with commercial  $\text{LiFePO}_4$  as cathode and Li metal as anode was charged by the TENG fabrics, FDSSC pack and the hybrid device for 10 min, respectively. The following discharge at  $1 \mu\text{A}$  lasted for 28, 59, and 98 min, respectively, further confirming the additive effect of the hybrid energy-harvesting textile (see Figure 6d). For all the three charging/discharging processes, the voltage of the battery increases to about 3.4 V rapidly during charge and has a stable 3.4 V plateau during discharge, correspondent with the characteristic of  $\text{LiFePO}_4$  cathode materials. It is worth noting that the LIB can be designed into flexible device, as shown by the flexible battery belt in our previous work.<sup>[24]</sup> Here, coin cell was used for convenience since the major focus of this work is improving the output of the energy-generating textile by integrating the TENG fabrics and fiber solar cells. The materials cost of the FDSSC and the TENG fabrics is estimated to be about  $\$0.5 \text{ cm}^{-1}$  and  $\$5 \text{ m}^{-2}$ , respectively, based on the raw materials used in our lab, confirming the materials viability and cost-effectiveness of the integrated power-textile.

Despite the advantages we demonstrated for the integrated energy-harvesting textile, there are still remaining challenges for future studies in order to commercialize our proposed power-textile: (1) further improvement of the average power output of the energy-generating textile; (2) developing miniature or flexible power management circuits for the whole energy-generating/storing systems; (3) long-term mechanical durability of the integrated energy harvesting textiles needs to be evaluated in the real application (on the

human body), which has more complicated mechanical deformations. Meanwhile, the design of the integrated power-textile should consider the function and mechanical durability of each energy-generating device, i.e., FDSSC might be designed into parts that have less mechanical deformation but more sunshine exposure, and TENG fabrics are placed on moving parts of human body.

In summary, a hybrid energy-harvesting power-textile was realized by integrating TENG fabrics and FDSSCs to harvest both the energy of human motions and solar light. A grating-structured and sliding-mode TENG fabric was fabricated by a novel route of laser-scribing masking and ELD Ni plating. This TENG fabric was demonstrated to be soft, lightweight, flexible, washable, breathable, and therefore compatible for integration into common textiles. The output performances of the TENG fabrics were optimized by reducing the segment size, achieving a peak power density of  $3.2 \text{ W m}^{-2}$  at sliding speed of  $0.75 \text{ m s}^{-1}$ . The FDSSCs achieved an average PCE of 6% with

an average  $J_{sc}$  of 10.6 mA cm<sup>-2</sup> and an average  $V_{oc}$  of 0.6 V. By connecting the FDSSC pack and rectified TENG fabrics in parallel, the hybrid power-textile outputted current that is about the sum of each component. Finally, a self-charging system was demonstrated by charging a LIB with the hybrid power-textile.

## Experimental Section

**Fabrication of the TENG Fabrics:** Laser-scribing masking and ELD plating were utilized to fabricate TENG fabrics, as schemed in Figure S1 (Supporting Information). Commercial polyester textile sandwiched between two Kapton tapes was put underneath a computer-controlled commercial CO<sub>2</sub> laser for drawing interdigitated patterns on one side. The intensity of the laser was controlled to cut the top Kapton tape into mask but not to damage the sandwiched polyester textile. The polyester textile with Kapton mask then undergo the ELD plating of conformal Ni coating with a method as previously reported.<sup>[18]</sup> Three sets of TENG fabrics were fabricated with the segment width as 1, 2, and 4 mm, respectively. The length and gap of the segments were kept as 35 and 0.5 mm, respectively. The area of the three TENG fabrics was about the same.

**Fabrication of the Fiber-Shaped Dye-Sensitized Solar Cells:** The FDSSCs were fabricated according to previous reports.<sup>[11]</sup> Briefly, the Ti wires with the diameter of 250 μm were dip-coated in TiO<sub>2</sub> suspensions until about 15 μm layer thickness was obtained. After being sintered at 450 °C for 30 min, the electrodes were sensitized with 0.5 × 10<sup>-3</sup> M N719 (Dalian Heptachroma, China) in ethanol for 24 h. A Pt wire with the diameter of 50 μm serving as the counter electrode was twisted around the above fabricated photoanode. The electrodes were put into a transparent and flexible plastic tube having the inner diameter of 0.6 mm and outer diameter of 0.7 mm. The tube was filled with an electrolyte solution in acetonitrile that contained 0.5 M 1,3-dimethylimidazolium iodide, 0.03 M I<sub>2</sub>, 0.05 M LiClO<sub>4</sub>, 0.5 M 4-tert-butylpyridine, and 0.05 M guanidine thiocyanate, followed by being sealed with glue.

**Measurement of the Output of the TENG Fabrics and FDSSCs:** The outputs of three sets of TENG fabrics at different sliding speeds were measured with a linear motor as the mechanical motion source. The output short-circuit current and open-circuit voltage of the TENG fabrics were measured by a Stanford low-noise current preamplifier (Model SR570) and an oscilloscope (LeCroy HDO6104), respectively. Current-voltage characteristics of FDSSCs were measured by an electrochemical workstation (Zahner, Zennium) under a solar simulator (Crowntech, SOL02 series).

**Battery Charge:** Seven FDSSCs were connected in series to obtain an open voltage of about 5 V and a short-circuit current of about 20 μA. Then, a pair of TENG fabrics with 1 mm wide segment rectified by a rectifier was connected with the FDSSCs pack in parallel to charge a 2032 type LIB coin cell composed of LiFePO<sub>4</sub> (Shenzhen Kejingstar Technology, LTD.) as the cathode and Li metal as the anode. The cathode was made by casting a film of LiFePO<sub>4</sub>, carbon black, and polyvinylidene fluoride (weight ratio is 8:1:1) on Al foil. The LIB coin cell was fabricated in an Ar-filled glovebox with both the content of oxygen and water less than 1 ppm. The TENG fabrics and FDSSCs were sewed onto the common clothes, and the connection wires, rectifier, and LIB coin cell were attached onto the clothes. For the battery charge, FDSSC pack was illuminated with the above solar simulator; the TENG fabric was slid by hands. The voltage was recorded by a Keithley electrometer (Keithley 6514). After the charge, a battery cycler (LAND CT2001A) was used to discharge the battery at 1 μA constant current.

## Supporting Information

Supporting Information is available from the Wiley Online Library or from the author.

## Acknowledgements

X.P., W.X.S., and M.M.L. contributed equally to this work. For support, the authors thank the “Thousands Talents” Program for Pioneering Research and Innovation, China, the National Natural Science Foundation of China (Grant Nos. 51432005, 61574018, 5151101243, 51561145021, and 61404035) and the One Hundred Person Project of the Chinese Academy of science.

Received: May 19, 2016

Revised: June 22, 2016

Published online:

- [1] a) A. K. Yetisen, H. Qu, A. Manbachi, H. Butt, M. R. Dokmeci, J. P. Hinstroza, M. Skorobogatiy, A. Khademhosseini, S. H. Yun, *ACS Nano* **2016**, *10*, 3042; b) M. Stoppa, A. Chiolerio, *Sensors* **2014**, *14*, 11957.
- [2] B. S. Shim, W. Chen, C. Doty, C. Xu, N. A. Kotov, *Nano Lett.* **2008**, *8*, 4151.
- [3] Z. Zhang, K. Guo, Y. Li, X. Li, G. Guan, H. Li, Y. Luo, F. Zhao, Q. Zhang, B. Wei, Q. Pei, H. Peng, *Nat. Photonics* **2015**, *9*, 233.
- [4] M. A. El-Sherif, J. Yuan, A. Macdiarmid, *J. Intell. Mater. Syst. Struct.* **2000**, *11*, 407.
- [5] M. Rothmaier, M. Luong, F. Clemens, *Sensors* **2008**, *8*, 4318.
- [6] G. Paul, R. Torah, S. Beeby, J. Tudor, *Sens. Actuators A* **2014**, *206*, 35.
- [7] L. Hu, Y. Cui, *Energy Environ. Sci.* **2012**, *5*, 6423.
- [8] a) D. C. Zou, *Abstr. Pap. Am. Chem. Soc.* **2013**, 245,470; b) X. Fan, Z. Z. Chu, F. Z. Wang, C. Zhang, L. Chen, Y. W. Tang, D. C. Zou, *Adv. Mater.* **2008**, *20*, 592; c) W. Zeng, L. Shu, Q. Li, S. Chen, F. Wang, X.-M. Tao, *Adv. Mater.* **2014**, *26*, 5310.
- [9] a) M. Peng, K. Yan, H. W. Hu, D. H. Shen, W. X. Song, D. C. Zou, *J. Mater. Chem. C* **2015**, *3*, 2157; b) B. Liu, B. Liu, X. Wang, D. Chen, Z. Fan, G. Shen, *Nano Energy* **2014**, *10*, 99; c) L. Li, T. Zhai, Y. Bando, D. Golberg, *Nano Energy* **2012**, *1*, 91; d) X. Fang, Z. Yang, L. Qiu, H. Sun, S. Pan, J. Deng, Y. Luo, H. Peng, *Adv. Mater.* **2014**, *26*, 1694; e) J. K. Koh, J. Kim, B. Kim, J. H. Kim, E. Kim, *Adv. Mater.* **2011**, *23*, 1641.
- [10] T. Chen, S. Wang, Z. Yang, Q. Feng, X. Sun, L. Li, Z.-S. Wang, H. Peng, *Angew. Chem. Int. Ed.* **2011**, *50*, 1815.
- [11] a) W. Song, H. Wang, G. Liu, M. Peng, D. Zou, *Nano Energy* **2016**, *19*, 1; b) M. Peng, D. Zou, *J. Mater. Chem. A* **2015**, *3*, 20435.
- [12] a) M. Peng, X. Yu, X. Cai, Q. Y. Yang, H. W. Hu, K. Yan, H. Wang, B. Dong, F. R. Zhu, D. C. Zou, *Nano Energy* **2014**, *10*, 117; b) Y. P. Fu, Z. B. Lv, S. C. Hou, H. W. Wu, D. Wang, C. Zhang, Z. Z. Chu, X. Cai, X. Fan, Z. L. Wang, D. C. Zou, *Energy Environ. Sci.* **2011**, *4*, 3379.
- [13] a) Z. L. Wang, J. Chen, L. Lin, *Energy Environ. Sci.* **2015**, *8*, 2250; b) K. Y. Lee, J. Chun, J.-H. Lee, K. N. Kim, N.-R. Kang, J.-Y. Kim, M. H. Kim, K.-S. Shin, M. K. Gupta, J. M. Baik, S.-W. Kim, *Adv. Mater.* **2014**, *26*, 5037; c) L. Valentini, M. Cardinali, J. Kenny, *J. Polym. Sci. B Polym. Phys.* **2014**, *52*, 859; d) B. Meng, W. Tang, Z. H. Too, X. Zhang, M. Han, W. Liu, H. Zhang, *Energy Environ. Sci.* **2013**, *6*, 3235.
- [14] Z. L. Wang, *ACS Nano* **2013**, *7*, 9533.
- [15] S. Wang, S. Niu, J. Yang, L. Lin, Z. L. Wang, *ACS Nano* **2014**, *8*, 12004.
- [16] Z. Zhao, X. Pu, C. Du, L. Li, C. Jiang, W. Hu, Z. L. Wang, *ACS Nano* **2016**, *10*, 1780.
- [17] G. Zhu, Y. Su, P. Bai, J. Chen, Q. Jing, W. Yang, Z. L. Wang, *ACS Nano* **2014**, *8*, 6031.
- [18] T.-C. Hou, Y. Yang, H. Zhang, J. Chen, L.-J. Chen, Z. Lin Wang, *Nano Energy* **2013**, *2*, 856.



- [19] Y. Xie, S. Wang, S. Niu, L. Lin, Q. Jing, J. Yang, Z. Wu, Z. L. Wang, *Adv. Mater.* **2014**, *26*, 6599.
- [20] X.-S. Zhang, M.-D. Han, R.-X. Wang, B. Meng, F.-Y. Zhu, X.-M. Sun, W. Hu, W. Wang, Z.-H. Li, H.-X. Zhang, *Nano Energy* **2014**, *4*, 123.
- [21] a) S. Li, Q. Zhong, J. Zhong, X. Cheng, B. Wang, B. Hu, J. Zhou, *ACS Appl. Mater. Interfaces* **2015**, *7*, 14912; b) W. Seung, M. K. Gupta, K. Y. Lee, K.-S. Shin, J.-H. Lee, T. Y. Kim, S. Kim, J. Lin, J. H. Kim, S.-W. Kim, *ACS Nano* **2015**, *9*, 3501.
- [22] J. Zhong, Y. Zhang, Q. Zhong, Q. Hu, B. Hu, Z. L. Wang, J. Zhou, *ACS Nano* **2014**, *8*, 6273.
- [23] S. Jung, J. Lee, T. Hyeon, M. Lee, D.-H. Kim, *Adv. Mater.* **2014**, *26*, 6329.
- [24] X. Pu, L. Li, H. Song, C. Du, Z. Zhao, C. Jiang, G. Cao, W. Hu, Z. L. Wang, *Adv. Mater.* **2015**, *27*, 2472.
- [25] a) L. Zheng, Z.-H. Lin, G. Cheng, W. Wu, X. Wen, S. Lee, Z. L. Wang, *Nano Energy* **2014**, *9*, 291; b) Y. Wu, X. Zhong, X. Wang, Y. Yang, Z. L. Wang, *Nano Res.* **2014**, *7*, 1631.
- [26] X. Pu, L. Li, M. Liu, C. Jiang, C. Du, Z. Zhao, W. Hu, Z. L. Wang, *Adv. Mater.* **2016**, *28*, 98.
- [27] Y. Guo, K. Li, C. Hou, Y. Li, Q. Zhang, H. Wang, *ACS Appl. Mater. Interfaces* **2016**, *8*, 4676.
- [28] F.-R. Fan, L. Lin, G. Zhu, W. Wu, R. Zhang, Z. L. Wang, *Nano Lett.* **2012**, *12*, 3109.
- [29] W. Tang, C. B. Han, C. Zhang, Z. L. Wang, *Nano Energy* **2014**, *9*, 121.
- [30] a) S. Niu, S. Wang, Y. Liu, Y. S. Zhou, L. Lin, Y. Hu, K. C. Pradel, Z. L. Wang, *Energy Environ. Sci.* **2014**, *7*, 2339; b) S. Niu, Z. L. Wang, *Nano Energy* **2015**, *14*, 161; c) B. Meng, W. Tang, X. Zhang, M. Han, W. Liu, H. Zhang, *Nano Energy* **2013**, *2*, 1101.
- [31] S. Niu, Y. Liu, S. Wang, L. Lin, Y. S. Zhou, Y. Hu, Z. L. Wang, *Adv. Mater.* **2013**, *25*, 6184.
- [32] X. Pu, M. Liu, L. Li, C. Zhang, Y. Pang, C. Jiang, L. Shao, W. Hu, Z. L. Wang, *Adv. Sci.* **2015**, *3*, 1500255.
- [33] Q. Jing, Y. Xie, G. Zhu, R. P. S. Han, Z. L. Wang, *Nat. Commun.* **2015**, *6*, 8031.
- [34] V. Nguyen, R. Zhu, R. Yang, *Nano Energy* **2015**, *14*, 49.
- [35] Z.-H. Lin, G. Cheng, L. Lin, S. Lee, Z. L. Wang, *Angew. Chem. Int. Ed.* **2013**, *52*, 12545.
- [36] a) X. Cai, H. W. Wu, S. C. Hou, M. Peng, X. Yu, D. C. Zou, *ChemSusChem* **2014**, *7*, 474; b) Y. P. Fu, M. Peng, Z. B. Lv, X. Cai, S. C. Hou, H. W. Wu, X. Yu, H. Kafafy, D. C. Zou, *Nano Energy* **2013**, *2*, 537; c) Y. P. Fu, Z. B. Lv, S. C. Hou, H. W. Wu, D. Wang, C. Zhang, D. C. Zou, *Adv. Energy Mater.* **2012**, *2*, 37.
- [37] a) H. Pettersson, T. Gruszecki, *Sol. Energy Mater. Sol. Cells* **2001**, *70*, 203; b) M. Ikegami, J. Suzuki, K. Teshima, M. Kawaraya, T. Miyasaka, *Sol. Energy Mater. Sol. Cells* **2009**, *93*, 836.